Conduction Band Engineering of Half–Heusler Thermoelectrics Using Orbital Chemistry

Conduction Band Engineering of Half-Heusler Thermoelectrics Using Orbital Chemistry [†]

Shuping Guo,[abd] Shashwat Anand,[b] Madison K. Brod,[b] Yongsheng Zhang[*ac] and G. Jeffrey Snyder[*b]

Semiconducting half-Heusler (HH, XYZ) phases are promising thermoelectric materials owing to their versatile electronic properties. Because the valence band of half-Heusler phases benefits from the valence band extrema at several high-symmetry points in the Brillouin zone (BZ), it is possible to engineer better p-type HH materials through band convergence. However, the thermoelectric studies of n-type HH phases have been lagging behind since the conduction band minimum is always at the same high-symmetry point (X) in the BZ, giving the impression that there is little opportunity for band engineering. Here we study the n-type orbital phase diagram of 69 HHs, and show that there are two competing conduction bands with very different effective masses actually at the same X point in the BZ, which can be engineered to be converged. The two conduction bands are dominated by the d orbitals of X and Y atoms, respectively. The energy offset between the two bands depends on the difference in electron configuration and electronegativity of the X and Y atoms. Based on the orbital phase diagram, we provide the strategy to engineer the conduction band convergence by mixing the HH compounds with the reverse band offsets. We demonstrate the strategy by alloying VCoSn and TaCoSn. The $V_{0.5}Ta_{0.5}CoSn$ solid solution is predicted to have high conduction band convergence and corresponding significantly larger density-of-states effective mass than either VCoSn or TaCoSn. Our work indicates that analyzing the orbital character of band edges provides new insight into engineering thermoelectric performance of HH compounds.

1 Introduction

Half-Heusler (HH) compounds are promising functional materials, e.g. thermoelectrics[1], optoelectronics[2], spintronics[3] and topological insulators[4], because of their versatile and complex electronic properties, as well as good thermal and mechanical stability[5]. As shown in Fig. 1, the crystal structure of HH (with the XYZ stoichiometry) is composed of four face-centered-cubic (FCC) sublattices, with X, Y and Z atoms occupying at the (0, 0, 0), (0.25, 0.25, 0.25) and (0.5, 0.5, 0.5) positions, respectively. The (0.75, 0.75, 0.75) position leaves as the vacant.

[a]Key Laboratory of Materials Physics, Institute of Solid State Physics, HFIPS, Chinese Academy of Sciences, Hefei 230031, China. E-mail: yshzhang@theory.issp.ac.cn

[b]Department of Materials Science and Engineering, Northwestern University, Evanston, IL 60208, USA. E-mail: jeff.snyder@northwestern.edu

[c]Advanced Research Institute of Multidisciplinary Sciences, Qufu Normal University, Qufu, Shandong Province, 273165, China.

[d]Institute for Theoretical Solid State Physics, Leibniz IFW Dresden, 01069 Dresden, Germany.

When the constituent elements are valence balanced[6,7], the compounds generally exhibit semiconducting properties. Therefore, valence balanced HH family has long been used for practical high-temperature thermoelectric applications[8].

The thermoelectric performance is characterized by the figure of merit, zT, $zT = S^2\sigma T/(\kappa_e + \kappa_l)$, where S is the Seebeck coefficient, σ the electrical conductivity, κ_e the electronic thermal conductivity and κ_l the lattice contribution to the thermal conductivity. But the Seebeck coefficient and electrical conductivity are inversely coupled by carrier concentration[1]. Thus, improving Seebeck coefficient and electrical conductivity at the same time is a long-standing challenge. The electronic properties are primarily determined by weighted mobility[9], $\mu(m_d^*/m_e)^{3/2}$, where large m_d^* (density-of-states effective mass) is favorable for large Seebeck coefficient and high μ (charge carrier mobility) is essential for high electrical conductivity. Large band degeneracy can boost m_d^*[10,11] without changing carrier mobility, leading to high weighted mobility[9] and then high thermoelectric performance[12]. As a consequence, modifying the relative energy of band edges (band engineering) has been used extensively as an effective strategy to improve the performance of thermoelectric

materials [13] where band degeneracy (N_b) can be seen as a simple and effective descriptor for good electronic properties for thermoelectric applications.

There has been great interest in engineering the valence bands and improve the thermoelectric performance of HH compounds. As a result, the zT of p-type NbFeSb-based [14] HH is reported to be 1.5 at high temperature. These p-type HHs have valence bands with high valley degeneracy (e.g $N_v^L = 4$, $N_v^W = 6$) which contributes to its high power factor [15,16]. Consequently, several promising p-type HH candidates are found with large valence band degeneracy, like $N_b^L = 8$ (with two orbital degeneracy) for NbFeSb and TaFeSb [17] and $N_b^{L+\Gamma} = 10$ (not including the spin-orbit split off band at Γ) for ZrCoBi [18] leading to zTs of 1.5 and 1.4, respectively. In contrast, there are few promising n-type HH thermoelectric candidates reported. Benefiting from the intrinsically low lattice thermal conductivity (7 W m^{-1} K^{-1} at 300 K) rather than the band degeneracy ($N_v^X = 3$), ZrNiSn based compounds remain the best n-type HH with zT values up to about 1.5 [19]. At room temperature (300 K), the lattice thermal conductivity of HH compounds is usually larger than 20 W m^{-1} K^{-1}. [20] Interestingly, the pristine ZrNiSn compound already shows a relatively low lattice thermal conductivity, likely due to Ni interstitial defects [21] ($\sim$ 7 W m^{-1} K^{-1} at 300 K), and the additional defect engineering can further decrease it to $\sim$ 3 W m^{-1} K^{-1}. [22,23] However, the band engineering (such as the well-known band convergence and effective mass engineering) [12,24] which has been long-time ignored might be a good way to further improve the thermoelectric performance of n-type HH materials.

Engineering HH thermoelectric materials based on structural chemistry is an effective way to understand the underlying mechanisms and propose feasible guidelines for improvements [25]. For instance, identifying the atomic orbital contribution to the valence and conduction band edges, which mainly determine the electronic transport, can guide band engineering. Recently, Dylla et al. [26] studied the orbital constitutions of the valence band edges (presenting an orbital contribution diagram). Over 50 known HH compounds were sorted into three groupings distinguished by the location of the valence band edge (at Γ, L or W): the band extremum locating at Γ or L depends on which atom's d-orbitals (X or Y in XYZ Half Heusler) dominate the valence band edge, the band extremum can also be at W with high valley degeneracy ($N_v^W = 6$) when the Z atom's p-orbitals further contribute to the valence band edge. The energy offset between the L and Γ points shows a linear relationship with valence difference (group number) between the X and Y atoms. Also the electronegativity difference between X and Y atoms was found to adjust E_L-E_Γ but to a lesser degree. [26] The chemical trends give valuable guidelines to engineer band convergence as well as high valley degeneracy. Unlike the valence band where the maximum can be at different locations for different HH compounds, the conduction band is almost always a single band located at the X point in the Brillouin zone. This makes it look like there is little opportunity to use band convergence for the n-type thermoelectric enhancement.

In this work, we examine the conduction band edges in 69 HH semiconductors and find that there are actually two different conduction bands at X point, one dominated by the d-orbitals of the

X atom (X_2) and the other dominated by the d-orbitals of the Y atom (X_3). As a result, the energy offset (E_{X_3}-E_{X_2}) has linear relationship with the valence difference between the X and Y atoms. For isovalent compounds, electronegativity difference between X and Y atoms has the noticeable effect on the band energy difference (E_{X_3}-E_{X_2}). This casts new insight into engineering band convergence in n-type thermoelectric HH compounds, which is successfully demonstrated in the mixture of VCoSn and TaCoSn.
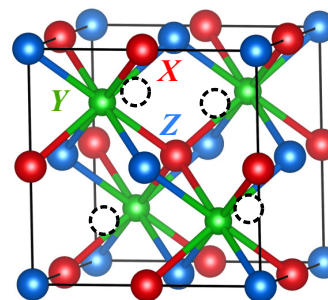
Fig. 1 Crystal structure of the half-Heusler compound. The red, green and blue spheres represent the X, Y and Z atoms, respectively. The black dotted circles represent the vacancies.

2 Methodology

2.1 Density Functional Theory

We use the projected augmented wave (PAW) [27] scheme with the generalized gradient approximation of Perdew-Burke-Ernzerhof (PBE) [28] electronic exchange correlation functional in the Vienna ab initio simulation package (VASP). The energy cutoff is $1.3E_{max}$ eV, where E_{max} is the largest energy of the default maximum energy cutoffs of X, Y and Z atoms. We use the Monkhorst-Pack [29] approach to sample the Brillouin zones with a roughly constant density of k-points (30 Å^3) for structure relaxation, and a highly dense density (60 Å^3) for electronic structure calculation. Since the spin-orbit coupling (SOC) induced energy band splitting is usually samller than several $k_B T$ in the HH compounds [18,30], such as the band splitting at Γ point for ZrCoBi is only 10 meV [18]. Bands with such small energy splitting can still be considered as the degenerate. Thus to avoid unnecessary computational cost, especially in the supercell structures, the spin-orbit coupling is omitted in our calculations. The conductivity effective mass (m_c^*) is calculated by Boltztrap2 [31] code for electrical conductivity using the constant relaxation time approximation (CRTA, $\tau = 10$ fs) [32].

$$(m_{c\alpha\beta}^*(T;\mu))^{-1} = \frac{\sigma_{\alpha\beta}(T;\mu)}{e^2\tau} \times \frac{1}{n(T;\mu)} \qquad (1)$$

2.2 Special Quasi-Random Structure (SQS) Method

Solid solutions are typically synthesized to lower the thermal conductivity [17,18] but can also affect the electronic properties [33]. To describe the disordered state, large supercells are needed, leading to time-consuming computational cost. Special quasi-random structures (SQS) [34] are chosen with close multisite correlation functions to the ideal disordered state in order to mimic the disorder of solid solution with a small supercell. SQS structures
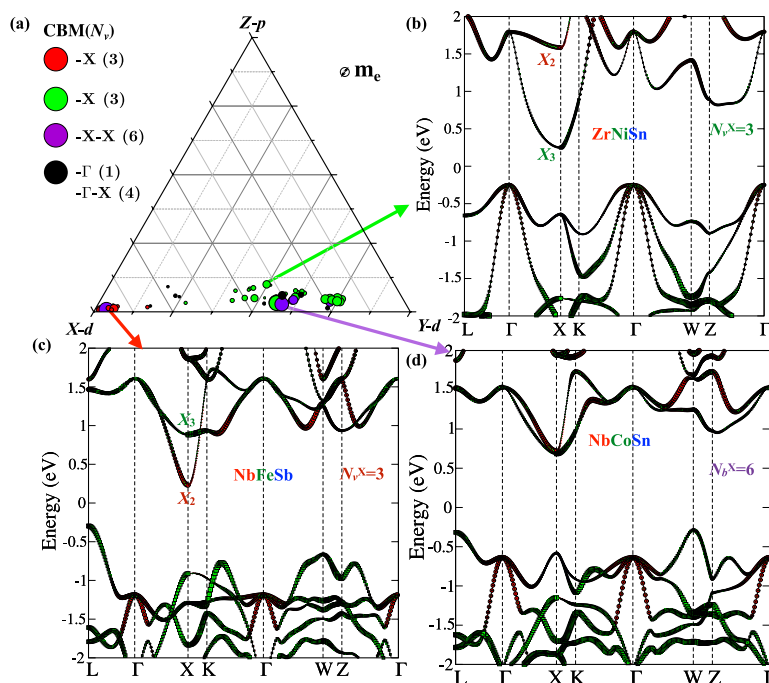
Fig. 2 (a) The conduction band edges of half-Heusler compounds are primarily composed of the d orbitals of the X and Y elements. The size of circles represents the n-type conductivity mass with the carrier concentration of 10^{20} cm^{-3} under 900 K. Two different conduction band minima (CBM) arise at the X point (valley degeneracy $N_v^X = 3$) in the Brillouin zone, one dominated by the d-orbital of X atoms (minimum at energy E_{X_2}, red sphere) and one dominated by the d-orbital of Y atoms (minimum at energy E_{X_3}, green sphere). In some compounds, such as ZrNiSn (b) the Y atom forms the CBM while in other compounds such as NbFeSb (c) the X atom forms the CBM. These two conduction bands are effectively converged in NbCoSn (d) with the energy difference of the CBMs being below a few $k_B T$, doubling the effective band degeneracy to 6 ($N_b^X = 6$).

have been successfully used to characterize the properties of experimental solid solutions, like ternary Sr-Pb-S[35], binary BCC alloys[36] as well as half-Heusler systems[11,37]. Wolverton[38] et al. predicted SQS structure with 48 atoms is used to study the V and Ta mixing in one of the FCC sublattices for the V$_{0.5}$Ta$_{0.5}$CoSn solid solution. To compare the band structures, BandUP[39] is used to unfold the band structure of the SQS into the primitive Brillouin zone of the pristine compound. The density-of-states (DOS) effective mass (m_d^*) of SQS-V$_{0.5}$Ta$_{0.5}$CoSn is calculated by fitting the DOS around the Fermi level.

$$DOS(E) = \frac{1}{2\pi^2}(\frac{2m_d^*}{\hbar^2})^{3/2}E^{1/2} \qquad (2)$$

3 Results and discussion

### 3.1 Orbital Diagram of Conduction Band Edges

Electronic structures provide important information relating to electronic transport properties. Band convergence leads to high DOS that increases the electronic quality factor[40] (or weighted mobility[9]) as long as there is not a proportional decrease in mobility, e.g. from intervalley scattering[41]. Engineering the band edges to achieve high band degeneracy is therefore a clear strategy to improve thermoelectric performance. A simple model is needed to engineer the band convergence by doping or alloying. Since the electronic states correspond to combinations of atomic orbitals, variations in the fractional contribution from each orbital type to a band should influence the band shape as well as the energy of the band edge.

The valence band edge of Half-Heusler semiconductors can be at Γ, the highest symmetry point in the Brillouin zone with $N_v^\Gamma = 1$, or at other points with higher valley degeneracy, like $N_v = 4$ at the L point and $N_v^W = 6$ at the W point[26]. But the conduction band edge is usually located at X (or sometimes Γ point), with valley degeneracy of $N_v = 3$. For the HH family, although each phase has the same crystal structure, it has wide chemistry flexibility since there are many possible elements for each site. Different elements result in different orbital contributions, leading to various band structures in HH compounds. Therefore, mapping the change of conduction band structures with various compositions of HH is a powerful strategy to elucidate the primary sources of variance among the reciprocal-space electronic structures.

To quantitatively explore how chemical composition (atomic orbitals) affect electronic structures, we select 69 kinds of stable (computationally stable at $T = 0$ K) HH compounds and project the density of states into the atomic orbitals, from which we can establish the conduction band orbital phase diagram. As shown in Fig. 2a, we can see that it is the contribution of d orbitals of the X and Y elements that mainly distinguish the conduction band edges. More importantly, although most HH compounds have conduction band edge at the X point there are actually two classes of conduction band edges. The conduction band minima of the both bands locate at the X point in BZ (Fig. 2b and 2c), one primarily arising from the d orbitals of X (red circles, making conduction band minimum at X_2) and another from Y atoms (green circles, making conduction band minimum at X_3). One representative of the second class is the well-known n-type HH ZrNiSn

(Fig. 2b): the conduction band minimum (CBM) locates at X point coming from the d orbital of Ni atom (green line, at X_3) and a secondary CBM at X point stemming from d orbital of Zr atom (red line, at X_2) with the energy difference (E_{X_3}-E_{X_2}) of -1.34 eV. In contrast, one representative of first class is the good p-type HH NbFeSb (Fig. 2c): the conduction band minimum is dominated by the Nb-d orbital (red line, X_2) and a secondary CBM attributed by the Fe-d orbital (green line, X_3), which are both laying on X point, with the energy offset (E_{X_3}-E_{X_2}) of 0.65 eV.

When the energy offset of these two types of CBM at X point (X_3 and X_2) is below a few k_BT, it implies that both two bands contribute to carrier transport, e.g. NbCoSn (Fig. 2d): the energy difference between X_3 and X_2 is 0.04 eV. In this case, the band degeneracy reaches six. The effective mass of X_2 (red line) is noticeably lighter than the X_3 (green line), indicating the coexistence of light and heavy band edges. ZrRhBi is another compound with effectively converged CBMs (Fig. S9d). There is a flat band between CBM-X_3 (contributed by d orbital of Y atom) and Γ point (ΔE = 0.03 eV), with the CBM-X_2 (attributed by d orbital of X atom) close in energy (ΔE = 0.25 eV), which should have a complex Fermi surface with high band degeneracy[42,43]. The orbital diversity of conduction band edges indicates larger degeneracy can be achieved by engineering the energy offset.
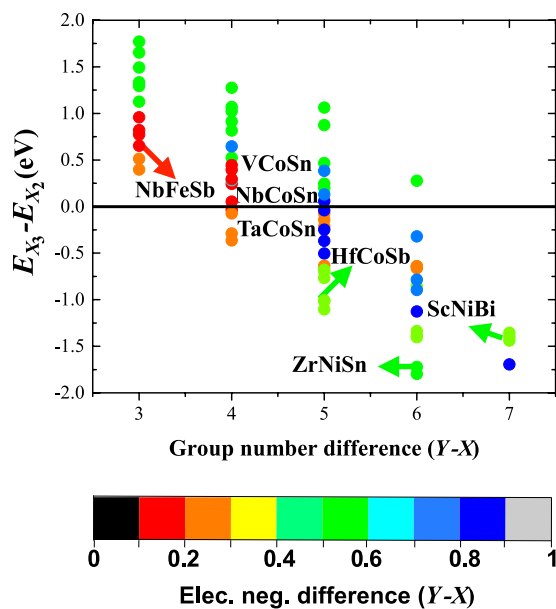

Fig. 3 The difference in valence electron configuration (group number) and electronegativity of X and Y species determines the energy offset between the two conduction bands at X (E_{X_3}-E_{X_2}) point.

3.2 Descriptor for Band Convergence of N-Type HH

Engineering the energy offset (E_{X_3}-E_{X_2}) to realize band degeneracy can tune thermoelectric performance, which depends on adjusting the relative energies of the atomic orbitals that constitute the conduction bands. Atomic orbitals from X, Y and Z atoms have bonding and anti-bonding interactions, which lead to the formation of the bands. It is reported that the simplified crystal orbital diagram for a prototypical half-Heusler compound

at X point, the competing CBMs are composed of either a non-bonding d-orbital states from the X atom and anti-bonding state comprised of mostly Y-d and X-d orbitals[44]. The chemical difference between X and Y atoms influences the relative energy difference between the atomic orbitals, and hence, the relative position of two distinct CBM at X point.

Fig. 3 shows the relationships between energy offset of two kinds of X points with valence electron configuration difference and electronegativity difference (color bar). The energy offset of E_{X_3} and E_{X_2} shows a linear relationship to the group number difference (the valance difference). Clearly, the valence electron difference, or the group or column number difference on the periodic table is a good descriptor for the energy difference. The variation in the relative energies of the two competing CBMs modified by group number difference between X and Y atoms is due to the increase in the on-site energy of the atomic orbitals moving across the row on the Periodic Table (left to right)[45]. Therefore, the compounds with a small valence difference, like NbFeSb, have the conduction band minimum (at X point with energy E_{X_2}) dominated by the d orbital of the X element. In contrast, compounds with large valence differences, such as HfCoSb, have the conduction band minimum (at X point with energy E_{X_3}) dominated by the d orbital of the Y atom. In this case, double mixing at X and Y sites with opposite energy offset (like NbFeSb and HfCoSb) can promote band convergence.
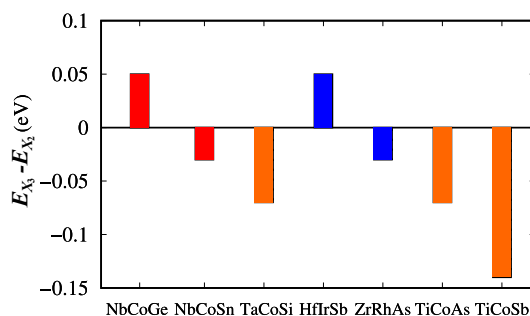
Fig. 4 The energy difference of E_{X_3}-E_{X_2} of seven compounds with small energy difference (near band convergence). The colors are the same as used in Figure 3, representing the electronegativity difference of X and Y species.

In addition, electronegativity, which characterizes the ionization energy of the element[46] has the secondary, but important, influence on the energies of the atomic orbitals. Therefore, for the isovalent compounds (like VCoSn and TaCoSn), the second most important descriptor is the difference of electronegativity between the X and Y atoms. The systems with smaller electronegativity differences (red and yellow solid circles in Fig. 3), which imply more covalent bonding, tend to reduce the E_{X_3}-E_{X_2} energy offset. The relationship between energy offset and these two descriptors can provide feasible guidance to engineer the band convergence. The energy offsets and projected band structures of all 69 HH compounds are given in Table S1 and Fig. S1-9, respectively.

When the group number differences are four and five, there are several systems with the energy offset below a few k_BT, which should effectively have both conduction bands converged. As
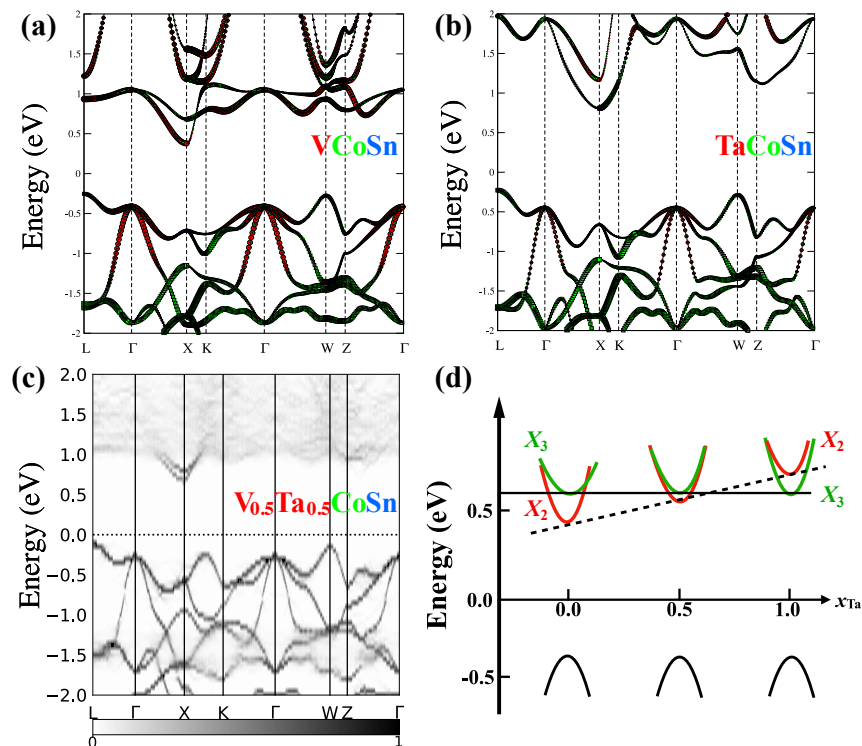
Fig. 5 The projected band structures of (a) VCoSn and (b) TaCoSn. Unfolded band structure of (c) $V_{0.5}Ta_{0.5}CoSn$ (SQS). The relative energy of the two conduction bands (X_2 and X_3) (d) changes with the doping concentration of Ta in $V_{1-x}Ta_xCoSn$ leading to band convergence near $x = 0.5$. The color bar is the special weight, which characterizes the probability of the primitive cell eignestates contributing to a particular supercell eigenstate of the same energy.

shown in Fig. 4, there are seven compounds (NbCoGe, NbCoSn, TaCoSi, HfIrSb, ZrRhAs, TiCoAs, TiCoSb) possess large band degeneracy of six with energy offset below a few k_BT. The colors are the same as used in Fig. 3, representing the difference of electronegativity. For other compounds with a large E_{X_3}-E_{X_2} energy offset, mixing two HH compounds with an opposite energy offset could also lead to band convergence.

3.3 Alloying to Achieve Conduction Band Convergence

From the last section, we can see that mixing two isovalent compounds with opposite energy offset can realize band degeneracy by tuning electronegativity difference. To validate this, we choose two isovalent systems (VCoSn and TaCoSn) with reverse energy offset to see how the changing of electronegativity can engineer the E_{X_3}-E_{X_2} energy offset. As shown in Fig. 5, the E_{X_3}-E_{X_2} energy offsets for VCoSn and TaCoSn are 0.30 and -0.36 eV, respectively. Based on a simple tight-bonding model[44,47], it can be shown that the on-site energy of an atomic orbital state affects the energy of the molecular orbital states which most closely resemble the atomic orbital state. That is, modifying the X-d orbital has a greater influence on the energy of the non-bonding CBM (E_{X_2}), while tuning the on-site energy of the Y-d atom has a greater influence on the anti-bonding CBM (E_{X_3}). Therefore, mixing Ta in VCoSn can increase the relative energy of X_2 then lead to the band convergence of X_2 and X_3. We choose SQS with the mixing concentrations of 50% Ta to study the electronic properties of solid solutions. In principle, the band structures of the SQS struc-

tures are very complicated due to the band (or Brillouin zone) folding. Therefore, to compare the complicated band structure of SQS to those using the pristine compounds, we have to unfold the band structure of the supercell into the original primitive Brillouin zone. Such band unfolding method has been widely used in defect investigations[35–37]. For $V_{0.5}Ta_{0.5}CoSn$ (Fig. 5c), the energy offset is around 0.15 eV, implying these two bands are converged with the degeneracy of six (Fig. 5d). It is clear that mixing V and Ta can modify the relative positions of X_2 and X_3. The convergence of light (X_2) and heavy (X_3) bands contributes to high DOS effective mass.
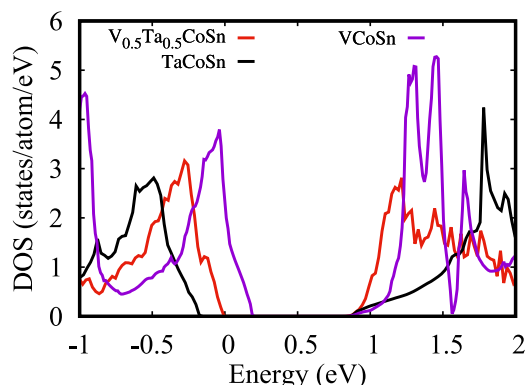
Fig. 6 Density-of-states of SQS-$V_{0.5}Ta_{0.5}CoSn$ (red line), VCoSn (purple line) and TaCoSn (black line).

We then calculate the density-of-states of $V_{0.5}Ta_{0.5}CoSn$, VCoSn and TaCoSn (Fig. 6). To check the DOS change with V-Ta mixing, we align their conduction band edges. It is clear that $V_{0.5}Ta_{0.5}CoSn$ has larger DOS around CBM than VCoSn and TaCoSn. Correspondingly, the DOS effective mass of $V_{0.5}Ta_{0.5}CoSn$ (3.49 m_e) is significantly higher than those of VCoSn (1.9 m_e) and TaCoSn (2.96 m_e). The high DOS effective mass of $V_{0.5}Ta_{0.5}CoSn$ is obviously contributed by the converged heavy and light bands, which is induced by the decreased E_{X_3}-E_{X_2} energy offset (Fig. 5c) in the mixture. Therefore, it would boost Seebeck coefficient without deteriorating the carrier mobility. Additionally, the introduced mass fluctuation (V and Ta) would scatter phonons and further suppress the lattice thermal conductivity as well. While there are some experimental studies on NbCoSn which should have high band degeneracy ($N_b^X = 6$)[48], our newly predicted candidate (the experimental unreported $V_{0.5}Ta_{0.5}CoSn$, $N_b^X = 6$) and others that may be selected using the same methods described here are promising strategies for future theoretical and experimental research. Therefore, engineering the conduction band convergence based on our methodology would essentially improve the thermoelectric performance of n-type HH compounds.

4 Conclusion

We construct the n-type orbital phase diagram with 69 compositions of half-Heusler XYZ compounds and find that there is orbital diversity of conduction band edges. Two major classes of conduction band edges (both at the X point) are dominated by the d orbitals of either the X (with energy E_{X_2}) or Y (with energy E_{X_3}) atom. The energy offset E_{X_3}-E_{X_2} is determined by the valence (group number in the periodic table) and electronegativity difference between X and Y species to a lesser extent. Mixing two pristine compounds (VCoSn and TaCoSn) with opposite energy offset in 1:1 ratio can successfully converge X_3 and X_2 bands. As a result, SQS-$V_{0.5}Ta_{0.5}CoSn$ exhibits a significantly higher n-type DOS effective mass than those of VCoSn and TaCoSn. Such an orbital diagram provides novel insight into understanding the underlying mechanisms behind the band energies and provides effective strategies to engineer high band degeneracy and better thermoelectric performance of half-Heusler compounds.

Acknowledgements

References

1 G. J. Snyder and E. S. Toberer, *Nat. Mater.*, 2008, **7**, 105–114.

2 D. Kieven, R. Klenk, S. Naghavi, C. Felser and T. Gruhn, *Phys. Rev. B*, 2010, **81**, 075208.

3 J. Ma, V. I. Hegde, K. Munira, Y. Xie, S. Keshavarz, D. T. Milde-brath, C. Wolverton, A. W. Ghosh and W. Butler, *Phys. Rev. B*, 2017, **95**, 024411.

4 H. Lin, L. A. Wray, Y. Xia, S. Xu, S. Jia, R. J. Cava, A. Bansil and M. Z. Hasan, *Nat. Mater.*, 2010, **9**, 546–549.

5 M. Al Malki, Q. Qiu, T. Zhu, G. Snyder and D. Dunand, *Mater. Today Phys.*, 2019, **9**, 100134.

6 T. Graf, C. Felser and S. S. Parkin, *Prog. Solid State Chem.*, 2011, **39**, 1–50.

7 S. Anand, K. Xia, V. I. Hegde, U. Aydemir, V. Kocevski, T. Zhu, C. Wolverton and G. J. Snyder, *Energy Environ. Sci.*, 2018, **11**, 1480–1488.

8 J.-W. G. Bos and R. A. Downie, *J. Phys.: Condens. Matter*, 2014, **26**, 433201.

9 G. J. Snyder, A. H. Snyder, M. Wood, R. Gurunathan, B. H. Snyder and C. Niu, *Adv. Mater.*, 2020, **32**, 2001537.

10 J. Xin, Y. Tang, Y. Liu, X. Zhao, H. Pan and T. Zhu, *npj Quant. Mater.*, 2018, **3**, 9.

11 Z. Liu, S. Guo, Y. Wu, J. Mao, Q. Zhu, H. Zhu, Y. Pei, J. Sui, Y. Zhang and Z. Ren, *Adv. Funct. Mater.*, 2019, **29**, 1905044.

12 Y. Pei, H. Wang and G. J. Snyder, *Adv. Mater.*, 2012, **24**, 6125–6135.

13 Y. Pei, X. Shi, A. LaLonde, H. Wang, L. Chen and G. J. Snyder, *Nature*, 2011, **473**, 66–69.

14 C. Fu, S. Bai, Y. Liu, Y. Tang, L. Chen, X. Zhao and T. Zhu, *Nat. commun.*, 2015, **6**, 8144.

15 S. Guo, T. Jia and Y. Zhang, *J. Phys. Chem. C*, 2019, **123**, 18824–18833.

16 Z. Feng, Y. Fu, A. Putatunda, Y. Zhang and D. J. Singh, *Phys. Rev. B*, 2019, **100**, 085202.

17 H. Zhu, J. Mao, Y. Li, J. Sun, Y. Wang, Q. Zhu, G. Li, Q. Song, J. Zhou, Y. Fu, R. He, T. Tong, Z. Liu, W. Ren, L. You, Z. Wang, J. Luo, A. Sotnikov, J. Bao, K. Nielsch, G. Chen, S. D. J. and Z. Ren, *Nat. commun.*, 2019, **10**, 270.

18 H. Zhu, R. He, J. Mao, Q. Zhu, C. Li, J. Sun, W. Ren, Y. Wang, Z. Liu, Z. Tang *et al.*, *Nat. Commun.*, 2018, **9**, 2497.

19 S. Sakurada and N. Shutoh, *Appl. Phys. Lett.*, 2005, **86**, 082105.

20 J. Carrete, W. Li, N. Mingo, S. Wang and S. Curtarolo, *Phys. Rev. X*, 2014, **4**, 011019.

21 H. Xie, H. Wang, Y. Pei, C. Fu, X. Liu, G. J. Snyder, X. Zhao and T. Zhu, *Adv. Funct. Mater.*, 2013, **23**, 5123–5130.

22 B. Gong, Y. Li, F. Liu, J. Zhu, X. Wang, W. Ao, C. Zhang, J. Li, H. Xie and T. Zhu, *ACS Appl. Mater. Interfaces*, 2019, **11**, 13397–13404.

23 N. S. Chauhan, P. R. Raghuvanshi, K. Tyagi, K. K. Johari, L. Tyagi, B. Gahtori, S. Bathula, A. Bhattacharya, S. D. Mahanti, V. N. Singh *et al.*, *J. Phys. Chem. C*, 2020, **124**, 8584–8593.

24 Y. Pei, A. D. LaLonde, H. Wang and G. J. Snyder, *Energy Environ. Sci.*, 2012, **5**, 7963–7969.

25 W. G. Zeier, J. Schmitt, G. Hautier, U. Aydemir, Z. M. Gibbs, C. Felser and G. J. Snyder, *Nat. Rev. Mater.*, 2016, **1**, 16032.

26 M. T. Dylla, A. Dunn, S. Anand, A. Jain and G. J. Snyder, *Research*, 2020, **2020**, 6375171.

27 G. Kresse and D. Joubert, *Phys. Rev. B*, 1999, **59**, 1758.

28 J. P. Perdew, K. Burke and M. Ernzerhof, *Phys. Rev. Lett.*, 1996, **77**, 3865.

29 H. J. Monkhorst and J. D. Pack, *Phys. Rev. B*, 1976, **13**, 5188.

30 G. Fiedler and P. Kratzer, *Phys. Rev. B*, 2016, **94**, 075203.

31 G. K. Madsen, J. Carrete and M. J. Verstraete, *Comput. Phys. Commun.*, 2018, **231**, 140–145.

32 Z. M. Gibbs, F. Ricci, G. Li, H. Zhu, K. Persson, G. Ceder, G. Hautier, A. Jain and G. J. Snyder, *npj Comput. Mater.*, 2017, **3**, 8.

33 H. Wang, A. D. LaLonde, Y. Pei and G. J. Snyder, *Adv. Funct. Mater.*, 2013, **23**, 1586–1596.

34 A. Zunger, S.-H. Wei, L. Ferreira and J. E. Bernard, *Phys. Rev. Lett.*, 1990, **65**, 353.

35 S. Hao, L.-D. Zhao, C.-Q. Chen, V. P. Dravid, M. G. Kanatzidis and C. M. Wolverton, *J. Am. Chem. Soc.*, 2014, **136**, 1628–1635.

36 C. Jiang, C. Wolverton, J. Sofo, L.-Q. Chen and Z.-K. Liu, *Phys. Rev. B*, 2004, **69**, 214202.

37 S. Guo, Z. Liu, Z. Feng, T. Jia, S. Anand, G. J. Snyder and Y. Zhang, *J. Mater. Chem. A*, 2020, **8**, 23590–23598.

38 C. Wolverton, *Acta Mater.*, 2001, **49**, 3129–3142.

39 P. V. Medeiros, S. Stafström and J. Björk, *Phys. Rev. B*, 2014, **89**, 041407.

40 X. Zhang, Z. Bu, X. Shi, Z. Chen, S. Lin, B. Shan, M. Wood, A. H. Snyder, L. Chen, G. J. Snyder *et al.*, *Sci. Adv.*, 2020, **6**, eabc0726.

41 J. Park, M. Dylla, Y. Xia, M. Wood, G. J. Snyder and A. Jain, *Nat. Commun.*, 2021, **12**, 3425.

42 M. T. Dylla, S. D. Kang and G. J. Snyder, *Angew. Chemie*, 2019, **131**, 5557–5566.

43 M. K. Brod and G. J. Snyder, *J. Mater. Chem. A*, 2021, **9**, 12119–12139.

44 J. C. Slater and G. F. Koster, *Phys. Rev.*, 1954, **94**, 1498.

45 W. A. Harrison, *Electronic structure and the properties of solids: the physics of the chemical bond*, Courier Corporation, 2012.

46 W. G. Zeier, A. Zevalkink, Z. M. Gibbs, G. Hautier, M. G. Kanatzidis and G. J. Snyder, *Angew. Chem. Int. Ed*, 2016, **55**, 6826–6841.

47 G. S. Rohrer, *Structure and bonding in crystalline materials*, Cambridge University Press, 2001.

48 F. Serrano-Sánchez, T. Luo, J. Yu, W. Xie, C. Le, G. Auffermann, A. Weidenkaff, T. Zhu, X. Zhao, J. A. Alonso *et al.*, *J. Mater. Chem. A*, 2020, **8**, 14822–14828.